A compact subcell WENO limiting strategy using immediate neighbors for Runge-Kutta discontinuous Galerkin methods for unstructured meshes

S R Siva Prasad Kochi[1]   and   M Ramakrishna[2]
siva.ksr@gmail.com   krishna@ae.iitm.ac.in

[1]Doctoral Candidate, Dept. of Aerospace Engg., IIT Madras.
[2]Professor, Dept. of Aerospace Engg., IIT Madras.

June 14, 2021

Abstract

In this paper, we generalize the compact subcell weighted essentially non oscillatory (CSWENO) limiting strategy for Runge-Kutta discontinuous Galerkin method developed recently in [1] for structured meshes to unstructured triangular meshes. The main idea of the limiting strategy is to divide the immediate neighbors of a given cell into the required stencil and to use a WENO reconstruction for limiting. This strategy can be applied for any type of WENO reconstruction. We used the WENO reconstruction proposed in [2] and provided accuracy tests and results for two-dimensional Burgers' equation and two dimensional Euler equations to illustrate the performance of this limiting strategy.

Keywords: discontinuous Galerkin method, WENO limiter, unstructured meshes

1   Introduction

In this paper, we look at the solution of hyperbolic conservation laws with the Runge-Kutta discontinuous Galerkin (RKDG) method [3] on unstructured meshes. To control spurious oscillations near discontinuities, a limiter is used. For higher orders, weighted essentially non oscillatory (WENO) limiters are preferred as they maintain the order of the scheme. We generalize the WENO limiting strategy developed recently in [1] for structured meshes to unstructured triangular meshes. This strategy works with any type of WENO reconstruction in the target cell using only the immediate neighbors by dividing them into subcells to obtain the required stencil. We used the WENO reconstruction proposed in [2] as it is quite simple for implementation.

WENO limiting for RKDG method was first presented by Qiu and Shu for structured meshes in [4]. Their limiter was extended to unstructured meshes by Zhu et al. in [5]. This limiter requires neighbors of neighbors for limiting in a given cell for higher orders. Various other limiters given in [6], [7], [8] addressed this issue of using a wide stencil and used the polynomial in a given cell along with the polynomials of the immediate neighbors to obtain a limited polynomial using WENO reconstruction. On the other hand, Dumbser et al [9] used a different strategy where the target cell is divided into subcells and an *a posteriori* limiting strategy is used. This was further refined using an Adaptive Mesh Refinement (AMR) technique by Giri and Qiu in [10].

We extend the compact limiting strategy used in [1] to unstructured meshes. Here, we use the immediate neighbors for limiting in a given cell and these neighbors are divided into subcells for higher order limiting. We assign appropriate values to these subcells as explained in Section 3. This limiting strategy can be used with any type of WENO reconstructions as given in [11] (called type-I WENO reconstruction), or [5] (called type-II WENO reconstruction) or [12] (mixed reconstruction) or the more recent methods given in [13] and [2]. WENO schemes form a weighted combination of several local reconstructions based on different stencils (called small stencils) and use it as the final WENO reconstruction. Type-I reconstruction consists of WENO schemes whose order of accuracy is not higher than that of the reconstruction on each small stencil. These schemes require very wide stencils for higher orders. On the other hand, type-II WENO schemes require smaller stencils whose order of accuracy is higher than that of the reconstruction on each small stencil. Each of these reconstructions have their

pros and cons and they are discussed in detail in [12]. We use the WENO reconstruction given by Zhu and Shu in [2] as it is quite simple in implementation and extension to higher orders is easy. These [2] schemes have linear weights that can be any positive numbers on the condition that their sum is one and number of spatial stencils is smaller than that of the same order accurate classical finite volume WENO schemes [14] on triangular meshes. We emphasize that our procedure works with any of the WENO reconstructions listed above by dividing the neighbors of the cell in which limiting is needed as is required by the reconstruction. We call this limiting strategy as compact subcell WENO limiter or CSWENO limiter in short.

The paper is organized as follows. We describe the formulation of the discontinuous Galerkin method used for all our results in Section 2, the proposed limiting procedure is described in Section 3 and the testing of the limiter and the results are described in Section 4 and finally we conclude the paper in Section 5.

2 Formulation of discontinuous Galerkin method on unstructured meshes

Consider a two-dimensional conservation law of the form for variable u

$$\frac{\partial u}{\partial t} + \frac{\partial f(u)}{\partial x} + \frac{\partial g(u)}{\partial y} = 0, \qquad x, y \in \mathbf{D} \tag{1}$$

with the initial condition at $t = 0$ given by,

$$u(x, y, 0) = u_0(x, y),$$

and the appropriate boundary conditions on the boundary $\partial \mathbf{D}$. Here $f(u)$ and $g(u)$ are fluxes in x and y directions respectively.

We assume that the domain $\mathbf{D}$ can be triangulated by K elements as

$$\mathbf{D} = \bigcup_{k=1}^{K} \mathbf{I}_k \tag{2}$$

where $\mathbf{I}_k$ is a straight sided triangle and the triangulation is assumed to be geometrically conforming i.e., $\partial \mathbf{D}$ is approximated by a piece wise linear polygon with each line a face of the triangle.

We approximate the local solution as a polynomial of order N as given by:

$$u_h^k(x, y, t) = \sum_{n=0}^{N_p-1} \hat{u}_n^k(t) \psi_n^k(x, y) \qquad \forall x, y \in \mathbf{I}_k \tag{3}$$

where $\psi_n^k(x, y)$ is a two dimensional polynomial basis of order N, N_p is the number of degrees of freedom and h is the size of the grid (which is in general the average of the lengths of the sides of the triangle). This is termed to be $\mathbf{P}^N$ based discontinuous Galerkin method whose formal order of accuracy is $N+1$. The number of degrees of freedom N_p is given by:

$$N_p = \frac{(N+1)(N+2)}{2}$$

We use the orthonormal basis as given in [15] for a standard isoparametric triangle I such that

$$I = \{\vec{r} = (r, s) | (r, s) \geq -1; r + s \leq 0\} \tag{4}$$

The basis is given as:

$$\psi_m(\vec{r}) = \sqrt{2} \left[P_i(a) P_j^{(2i+1,0)}(b) \right] (1-b)^i \tag{5}$$

where

$$m = j + (N+1)i + 1 - \frac{i}{2}(i-1), \qquad (i,j) \geq 0; \qquad i + j \leq N$$

and

$$a = 2\frac{1+r}{1-s} - 1; \qquad b = s$$

and $P_n^{(\alpha,\beta)}(x)$ is the nth order Jacobi polynomial.

We approximate the fluxes $f(u(x,y,t),x,y,t)$ and $g(u(x,y,t),x,y,t)$ in the domain $\mathbf{D}$ as

$$f_h^k(u_h^k) = \sum_{n=0}^{N_p-1} \hat{f}_n^k(t)\psi_n^k(x,y) \qquad \forall x,y \in \mathbf{I}_k \tag{6}$$

$$g_h^k(u_h^k) = \sum_{n=0}^{N_p-1} \hat{g}_n^k(t)\psi_n^k(x,y) \qquad \forall x,y \in \mathbf{I}_k \tag{7}$$

where $\hat{f}_n^k(t) = f(\hat{u}_n^k(t))$ and $\hat{g}_n^k(t) = g(\hat{u}_n^k(t))$. Substituting equations (3), (6) and (7) in (1) and integrating it by parts, we get the following scheme to advance the degrees of freedom $\hat{u}_n^k(t)$ in time in an element given by $\mathbf{I}_k = [x_l^k, y_l^k] \times [x_r^k, y_r^k]$:

$$\frac{d}{dt}\hat{u}_h^k = (\mathbf{M}^k)^{-1}(\mathbf{S_x}^k)^T \hat{f}_h^k(\hat{u}_h^k) + (\mathbf{M}^k)^{-1}(\mathbf{S_y}^k)^T \hat{g}_h^k(\hat{u}_h^k) \tag{8}$$
$$-(\mathbf{M}^k)^{-1}(f^*|_{r_{N_p}} e_{N_p} - f^*|_{r_1} e_1) - (\mathbf{M}^k)^{-1}(g^*|_{s_{N_p}} e_{N_p} - g^*|_{s_1} e_1) = L(u_h^k)$$

Here, $\hat{u}_h^k = [\hat{u}_0^k \ldots \hat{u}_{N_p-1}^k]^T$, e_i is a vector of dimension N_p which has zero entries everywhere except at the ith location and $\mathbf{M}^k$ is the local mass matrix which is given as:

$$\mathbf{M}^k = [M_{ij}^k] = \left[\int_{\mathbf{I}_k} \psi_i^k(x,y)\psi_j^k(x,y) \, \mathrm{dA} \right] \tag{9}$$

and $\mathbf{S_x}^k$ and $\mathbf{S_y}^k$ are the local stiffness matrices given by:

$$\mathbf{S_x}^k = [S_{xij}^k] = \left[\int_{\mathbf{I}_k} \psi_i^k(x,y)\frac{\partial\psi_j^k(x,y)}{\partial x} \, \mathrm{dA} \right] \tag{10}$$

$$\mathbf{S_y}^k = [S_{yij}^k] = \left[\int_{\mathbf{I}_k} \psi_i^k(x,y)\frac{\partial\psi_j^k(x,y)}{\partial y} \, \mathrm{dA} \right] \tag{11}$$

Also, f^* and g^* are the x and y components of the monotone numerical flux at the interface which is calculated using an exact or approximate Riemann solver. We have used the Lax-Friedrichs flux for all the test cases given below.

3   Proposed limiting procedure on unstructured meshes

In this section, we describe the details of the proposed limiting procedure using WENO reconstruction and the division of cells into subcells for the discontinuous Galerkin method. This step is a generalization of the procedure in [1] for structured meshes. The common method for limiting in discontinuous Galerkin method is:
1) Identify the cells which need to be limited, known as troubled cells.
2) Replace the solution polynomial in the troubled cell with a new polynomial that is less oscillatory but with the same cell average and order of accuracy.

For the first step, we have used the KXRCF troubled cell indicator [16] for all the calculations done

in this paper as it is rated highly by Qiu and Shu in [17] on the basis of it's performance in detecting the discontinuities in various test problems. We give a brief description of the troubled cell indicator in the following subsection.

3.1 KXRCF Troubled cell indicator

The troubled cell indicator used in this work was developed by Krivodonova et al. [16]. This indicator is termed as KXRCF troubled cell indicator by using the names of the authors of the paper [16].

For a given problem, partition the boundary $\partial \mathbf{I}_j$ of a given cell $\mathbf{I}_j$ into portions $\partial \mathbf{I}_j^-$ and $\partial \mathbf{I}_j^+$ where the flow is into $(\bar{v}.\bar{n} < 0)$ and out of $(\bar{v}.\bar{n} > 0)$ $\mathbf{I}_j$, respectively. For the scalar conservation laws, $\bar{v}$ is taken to be $(f'(u), g'(u))$ and for the Euler equations it is the velocity vector. The troubled cell indicator is defined as

$$R_j = \frac{|\int_{\partial \mathbf{I}_j^-} (U_j - U_{nbj}) ds|}{h^{(N+1)/2} |\partial \mathbf{I}_j^-| \ \ ||U_j||} \tag{12}$$

where U_j is the discontinuous Galerkin value of u on $\mathbf{I}_j$, U_{nbj} the value across the boundary, $||U_j||$ the standard L^2 norm in the cell $\mathbf{I}_j$ and N is the order of the polynomial basis. We take h to be the radius of the circumscribed circle in $\mathbf{I}_j$. Now if $R_j > C_K$, $\mathbf{I}_j$ is identified to be a troubled cell. We take C_K to be 1.

3.2 Limiting procedure

After identifying the troubled-cells, we would like to reconstruct the values of $\hat{u}_n^j$ for the troubled-cell $\mathbf{I}_j$ for $n = 1, \ldots, N_p - 1$. That is, we retain the cell average $\hat{u}_0^j$ and reconstruct all the other degrees of freedom. To do that, we use the quadrature points given in [18] (SCP-quadrature) and find the solution at those points using WENO reconstruction. These quadrature points are termed as (x_q, y_q) for $q = 0, \ldots, N_p - 1$. We can use any of the WENO reconstructions given in [11] (called type I WENO reconstruction), or [5] (called type II WENO reconstruction) or [12] (mixed reconstruction) or the more recent methods given in [13] and [2]. WENO schemes form a weighted combination of several local reconstructions based on different stencils (called small stencils) and use it as the final WENO reconstruction. Type-I reconstruction consists of WENO schemes whose order of accuracy is not higher than that of the reconstruction on each small stencil. These schemes require very wide stencils for higher orders. On the other hand, type-II WENO schemes require smaller stencils whose order of accuracy is higher than that of the reconstruction on each small stencil. But, they sometimes require negative linear weights and do not work properly for geometries of poor mesh quality. Each of these reconstructions have their pros and cons and they are discussed in detail in [12]. We use the WENO reconstruction given by Zhu and Shu in [2] as it is quite simple in implementation and extension to higher orders is easy. These [2] schemes have linear weights that can be any positive numbers on the condition that their sum is one and number of spatial stencils is smaller than that of the same order accurate classical finite volume WENO schemes [14] on triangular meshes. We emphasize that our procedure works with any of the WENO reconstructions listed above by dividing the neighbors of the cell in which limiting is needed as is required by the reconstruction. For the $\mathbf{P}^1$ based DGM, we now describe the procedure for the reconstruction of the moments $\hat{u}_1^k$ and $\hat{u}_2^k$ in the troubled cell $\mathbf{I}_j$ using the WENO reconstruction procedure for triangles. We relabel the troubled cell as Δ_0 and its immediate neighbors as Δ_1, Δ_2 and Δ_3 as shown in Figure 1 where they are labeled according to their subscripts.
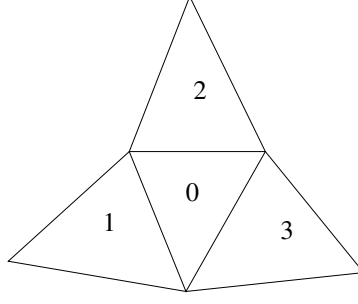
Figure 1: Troubled Cell and its immediate neighbors

For a third order WENO reconstruction, we also need the neighbors of the cells Δ_1, Δ_2 and Δ_3 as suggested in [5]. Instead of using their actual neighbors, we divide each of those triangles into three equal parts by joining the centroid of a triangle to its vertices as shown in Figure 2a. Now, we get the new stencil required for the third order WENO reconstruction. Now, we use the DG local polynomial for Δ_1 and take its average in the new cells Δ_{11}, Δ_{12} and Δ_{13} to obtain the cell averages for the new cells. Similarly, we can calculate the cell average for the cells Δ_{21}, Δ_{22}, Δ_{23}, Δ_{31}, Δ_{32} and Δ_{33} using the DG local polynomial of cells Δ_2 and Δ_3. We can use the same procedure to divide the neighboring cells for $\mathbf{P}^N$ based DGM for any N based on the required number of quadrature points. As the order of the polynomial increases, the number of triangles required to maintain the order of the scheme increases. We split the neighbors in such a way that this will not reduce the order of accuracy as explained in [14].
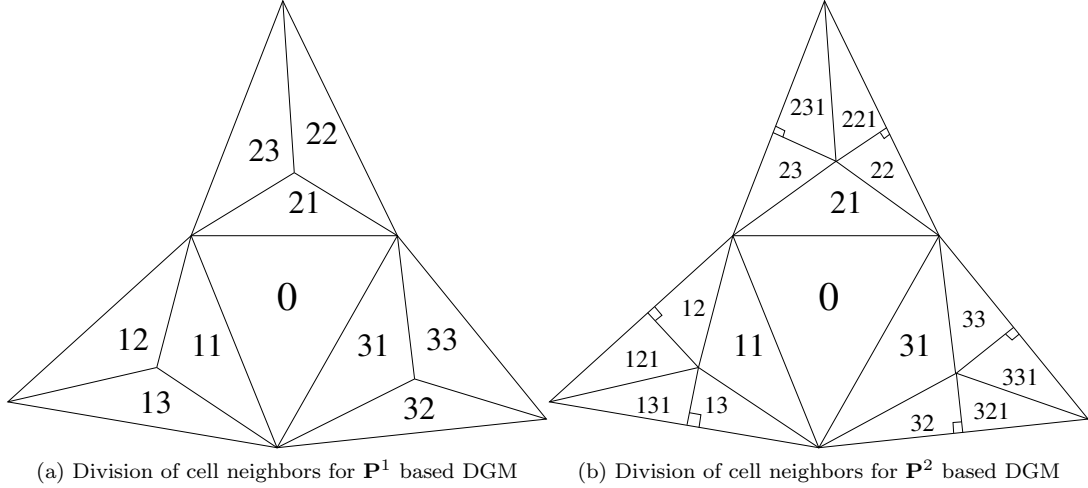

(a) Division of cell neighbors for $\mathbf{P}^1$ based DGM

(b) Division of cell neighbors for $\mathbf{P}^2$ based DGM

Figure 2: Division of cell neighbors for WENO reconstruction using $\mathbf{P}^1$ and $\mathbf{P}^2$ based DGM
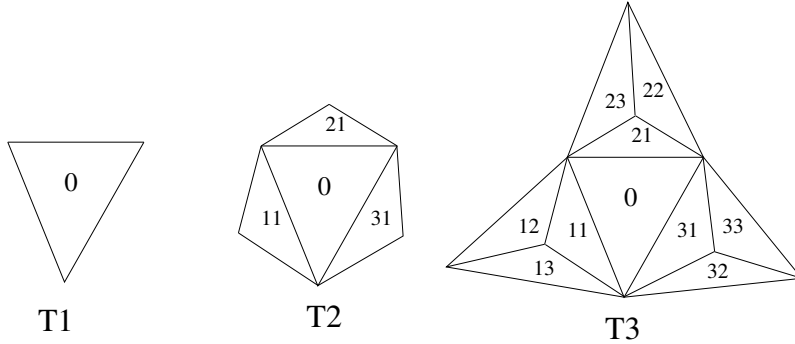

Figure 3: Required stencils for $\mathbf{P}^1$ based DGM

Now the step by step WENO reconstruction procedure to be used for $\mathbf{P}^1$ based DGM is described below:

Step 1: We use stencils T1, T2 and T3 as shown in Figure 3 for WENO reconstruction. For T1 $= \{\Delta_0\}$, we assign a zeroth order polynomial $q_1(x,y) = \hat{u}_0^j$. Now on T2 $= \{\Delta_0, \Delta_{11}, \Delta_{21}, \Delta_{31}\}$, we obtain a linear polynomial $q_2(x,y)$ such that it has the same cell average as u on the troubled cell Δ_0 and matches the cell averages of u (obtained earlier) on the other triangular cells in the set T2$\backslash\{\Delta_0\}$ in a least square sense [14]. To obtain a quadratic polynomial $q_3(x,y)$, we use the stencil T3 $= \{\Delta_0, \Delta_{11}, \Delta_{21}, \Delta_{31}, \Delta_{12}, \Delta_{13}, \Delta_{22}, \Delta_{23}, \Delta_{32}, \Delta_{33}\}$ such that it has the same cell average as u on the troubled cell Δ_0 and matches the cell averages of u on the other triangular cells in the set T3$\backslash\{\Delta_0\}$ in a least square sense [14].

Step 2: Now, we obtain equivalent expressions for these polynomials $q_1(x,y)$, $q_2(x,y)$ and $q_3(x,y)$. We define:

$$p_1(x,y) = q_1(x,y) \tag{13}$$

$$p_2(x,y) = \frac{1}{\gamma_{2,2}} q_2(x,y) - \frac{\gamma_{1,2}}{\gamma_{2,2}} p_1(x,y) \quad \text{with} \quad \sum_{l=1}^{2} \gamma_{l,2} = 1 \quad \text{and} \quad \gamma_{2,2} \neq 0 \tag{14}$$

and

$$p_3(x,y) = \frac{1}{\gamma_{3,3}} q_3(x,y) - \sum_{l=1}^{2} \frac{\gamma_{l,3}}{\gamma_{3,3}} p_l(x,y) \quad \text{with} \quad \sum_{l=1}^{3} \gamma_{l,3} = 1 \quad \text{and} \quad \gamma_{3,3} \neq 0 \tag{15}$$

Here the $\gamma_{l,m}$ are linear weights. We choose them as in [2] as $\gamma_{l,m} = \bar{\gamma}_{l,m}/(\sum_{l=1}^{m} \bar{\gamma}_{l,m})$ with $\bar{\gamma}_{l,m} = (1/h)^{l-1}$, $l = 1, \ldots, t$ and $m = 2, 3$ $(t = m)$ where h is the grid size (which is in general the average of the lengths of the sides of the triangle). Here we changed the expression for $\bar{\gamma}_{l,m}$ from $\bar{\gamma}_{l,m} = 10^{l-1}$ (which is used in [2]) to $\bar{\gamma}_{l,m} = (1/h)^{l-1}$. This change was made so that $\gamma_{l,m} = O(h^{m-l})$. In this manner, we get larger linear weights for high degree polynomials and smaller linear weights for low degree polynomials. Also, using a Taylor series expansion of cell averages about the barycenter of the triangle Δ_0 as given in [19], we obtain $u(x_q, y_q) - p_l(x_q, y_q) = O(h^l)$, where $u(x_q, y_q)$ is the exact solution at the quadrature point q.

Step 3: We now compute the smoothness indicator for each stencil denoted by β_l for $l = 2, 3$. As given by [20], we use:

$$\beta_l = \sum_{|l|=1}^{N} |\Delta_0|^{|l|-1} \int_{\Delta_0} \left(\frac{\partial^{|l|}}{\partial x^{l_1} \partial x^{l_2}} p_i(x,y) \right)^2 dx dy, \quad l = 2, 3 \tag{16}$$

where $l = (l_1, l_2)$, $|l| = l1 + l2$. For β_1, we magnify it from 0 to a value defined in equation (18) as given by [2]. Using the stencils in Figure 3, we construct three polynomials $p_{1,l}(x,y) \in \text{span}\{\frac{x-x_l}{|\Delta_l|^{1/2}}\}$, $l = 1, 2, 3$, satisfying $p_{1,1}(x_{12}, y_{12}) = \bar{u}_{12} - \bar{u}_{11}$, $p_{1,1}(x_{13}, y_{13}) = \bar{u}_{13} - \bar{u}_{11}$, $p_{1,2}(x_{22}, y_{22}) = \bar{u}_{22} - \bar{u}_{21}$, $p_{1,2}(x_{23}, y_{23}) = \bar{u}_{23} - \bar{u}_{21}$, $p_{1,3}(x_{32}, y_{32}) = \bar{u}_{32} - \bar{u}_{31}$, $p_{1,3}(x_{33}, y_{33}) = \bar{u}_{33} - \bar{u}_{31}$, where (x_l, y_l) are centroids of Δ_l, $l = 11, 12, 13; 21, 22, 23; 31, 32, 33$, respectively. Now, we use equation (16) to find $\beta_{1,l}$, $l = 1, 2, 3$. We set $\lambda_{1,1} = \lambda_{1,2} = \lambda_{1,3} = 1/3$ and

$$\sigma_l = \lambda_{1,l} \left(1 + \frac{\left(\left[|\beta_{1,1} - \beta_{1,2}|^2 + |\beta_{1,2} - \beta_{1,3}|^2 + |\beta_{1,3} - \beta_{1,1}|^2 \right] /3 \right)^2}{\beta_{1,l} + \epsilon} \right), l = 1, 2, 3 \tag{17}$$

with $\sigma = \sigma_1 + \sigma_2 + \sigma_3$, where $\epsilon = 10^{-10}$. Then we get

$$\beta_1 = \sum_{|l|=1} |\Delta_0|^{|l|} \left(\frac{\partial^{|l|}}{\partial x^{l_1} \partial x^{l_2}} \left(\sum_{l=1}^{3} \frac{\sigma_l}{\sigma} p_{1,l}(x,y) \right) \right)^2 \tag{18}$$

Again using a Taylor series expansion of cell averages about the barycenter of the triangle Δ_0, we obtain for $l = 1, 2, 3$, $\beta_l = d(x_l, y_l)h^2(1 + O(h^2))$ for some function d where (x_l, y_l) is the location of barycenter of $\mathbf{I}_j$. If a particular stencil, say T2 is not smooth, then $\beta_2 = O(1)$.

Step 4: We compute the nonlinear weights using the WENO-Z recipe [21]. We first find τ using

$$\tau = \frac{|\beta_3 - \beta_1|^2 + |\beta_3 - \beta_2|^2}{4} \tag{19}$$

Here, using the Taylor series expansions about the barycenter of the triangle Δ_0, we obtain $\tau = O(h^6)$. Now, the nonlinear weights are given by

$$\omega_l = \frac{\bar{\omega}_l}{\sum_{l=1}^{3} \bar{\omega}_l}, \quad \bar{\omega}_l = \gamma_{l,3} \left(1 + \frac{\tau}{\epsilon + \beta_l} \right) \quad l = 1, 2, 3 \tag{20}$$

Again we take ϵ as 10^{-10}. Now assuming $\epsilon << \beta_l$, we get $\omega_1 - \gamma_{1,3} = O(h^6)$, $\omega_2 - \gamma_{2,3} = O(h^5)$, and $\omega_3 - \gamma_{3,3} = O(h^4)$. If a particular stencil, say T2 is not smooth, then $\omega_2 - \gamma_{l,2} = O(1)$. We note that the stencil T1 is always smooth as it contains only one cell with a given cell average. Now, we can write the final WENO approximation at the required quadrature point q as

$$u_q = \sum_{l=1}^{3} \omega_l p_l(x_q, y_q) \quad q = 0, \dots, N_p - 1 \tag{21}$$

Now, we write

$$u_q - u(x_q, y_q) = \omega_0 p_0(x_q, y_q) + \omega_1 p_1(x_q, y_q) + \omega_2 p_2(x_q, y_q) - u(x_q, y_q) \tag{22}$$

which can written as

$$
\begin{aligned}
u_q - u(x_q, y_q) = & [(\omega_3 - \gamma_{3,3})(p_3(x_q, y_q) - u(x_q, y_q))] + [(\omega_2 - \gamma_{2,3})(p_2(x_q, y_q) - u(x_q, y_q))] \\
& + [(\omega_1 - \gamma_{1,3})(p_1(x_q, y_q) - u(x_q, y_q))] + [\gamma_{3,3}(p_3(x_q, y_q) - u(x_q, y_q))] \\
& + [\gamma_{2,3}(p_2(x_q, y_q) - u(x_q, y_q))] + [\gamma_{1,3}(p_3(x_q, y_q) - u(x_q, y_q))]
\end{aligned} \tag{23}
$$

If all the stencils are smooth, from the right hand side of equation (23), we can see that $u(x_q, y_q) - u_q = O(h^3)$. If any one of the stencils (say T2) is not smooth, then $\omega_2 - \gamma_{2,3} = O(1)$ and the right hand side of equation (23) will become $O(h^2)$. This limit is the required order of accuracy for the reconstruction of moments for $\mathbf{P^1}$ based DGM.

Step 5: Finally, we obtain the reconstructed degrees of freedom based on the reconstructed point values u_q at the quadrature points (x_q, y_q) and a numerical integration as

$$\hat{u}_i^j = |\Delta_0| \sum_q w_q u_q \psi_i^j(x_q, y_q) \quad i = 1, \dots, N_p - 1 \tag{24}$$

where $|\Delta_0|$ is the area of Δ_0 and w_G's are the quadrature weights for the points (x_q, y_q) as given by [18].

For the $\mathbf{P^2}$ based DGM, the procedure to construct the second order moments $\hat{u}_1^k$, $\hat{u}_2^k$, $\hat{u}_3^k$, $\hat{u}_4^k$ and $\hat{u}_5^k$ in the troubled cell Δ_0 is similar to the above procedure. Here, we require some extra neighbors for the WENO reconstruction as we need a fifth order WENO reconstruction and they are shown in Figure 2b. Here note that the new triangles $221, 231$ etc., are obtained by dropping a perpendicular to the opposite side as required. The cell averages for the new cells are obtained using the same procedure described above for $\mathbf{P^1}$ based DGM. The WENO reconstruction procedure for this case is described below:
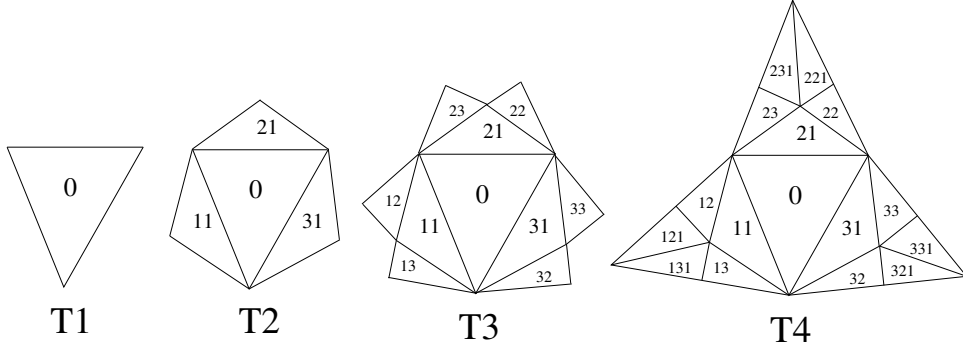
Figure 4: Required stencils for $\mathbf{P}^2$ based DGM

Step 1: We use stencils T1, T2, T3 and T4 as shown in Figure 4 for WENO reconstruction. We obtain $q_1(x,y)$, $q_2(x,y)$ and $q_3(x,y)$ using stencils T1, T2 and T3 as described in the procedure above. Now, using T4 = $\{\Delta_0, \Delta_{11}, \Delta_{21}, \Delta_{31}, \Delta_{12}, \Delta_{13}, \Delta_{121}, \Delta_{131}, \Delta_{22}, \Delta_{23}, \Delta_{221}, \Delta_{231}, \Delta_{32}, \Delta_{33}, \Delta_{321}, \Delta_{331}\}$, we obtain a cubic polynomial $q_4(x,y)$, such that it has the same cell average as u on the troubled cell Δ_0 and matches the cell averages of u on the other triangular cells in the set T4$\backslash\{\Delta_0\}$ in a least square sense. Again a quartic polynomial $q_5(x,y)$ is obtained on T5 such that it has the same cell average as u on the troubled cell Δ_0 and matches the cell averages of u on the other triangular cells in the set T4$\backslash\{\Delta_0\}$ in a least square sense.

Step 2: We obtain $p_1(x,y)$, $p_2(x,y)$ and $p_3(x,y)$ using equations (13), (14) and (15) respectively. We now define:

$$p_4(x,y) = \frac{1}{\gamma_{3,4}}q_4(x,y) - \sum_{l=1}^{2}\frac{\gamma_{l,4}}{\gamma_{3,4}}p_l(x,y) \quad \text{with} \quad \sum_{l=1}^{3}\gamma_{l,4} = 1 \quad \text{and} \quad \gamma_{3,4} \neq 0 \tag{25}$$

$$p_5(x,y) = \frac{1}{\gamma_{4,5}}q_5(x,y) - \sum_{l=1}^{3}\frac{\gamma_{l,5}}{\gamma_{4,5}}p_l(x,y) \quad \text{with} \quad \sum_{l=1}^{4}\gamma_{l,5} = 1 \quad \text{and} \quad \gamma_{4,5} \neq 0 \tag{26}$$

We choose $\gamma_{l,m}$ again as given above for $m = 2,3$. For $m = 4,5$, we set $\gamma_{l,m} = \bar{\gamma}_{l,m}/\left(\sum_{l=1}^{m}\bar{\gamma}_{l,m}\right)$ with $\bar{\gamma}_{l,m} = (1/h)^{l-1}$, $l = 1,\ldots,t$ and $m = 4,5$ ($t = m-1$) where h is the grid size.

Step 3: Using the same procedure given in Step 3 for $\mathbf{P}^1$ based DGM and equations (16), (18), we obtain β_l, for $l = 1,2,3,4,5$.

Step 4: We find τ required for calculating nonlinear weights using

$$\tau = \frac{|\beta_4 - \beta_1|^2 + |\beta_4 - \beta_2|^2 + |\beta_4 - \beta_3|^2}{16} \tag{27}$$

Now, we calculate the nonlinear weights using

$$\omega_l = \frac{\bar{\omega}_l}{\sum_{l=1}^{4}\bar{\omega}_l}, \quad \bar{\omega}_l = \gamma_{l,5}\left(1 + \frac{\tau}{\epsilon + \beta_l}\right) \quad l = 1,2,3,4 \tag{28}$$

Again we take ϵ as 10^{-10}. Now, we can write the final WENO approximation at the required quadrature point q as

$$u_q = \sum_{l=1}^{4}\omega_l p_l(x_q, y_q) \quad q = 0,\ldots,N_p - 1 \tag{29}$$

Using equations (29) and (23), we can say that when the solution of smooth, $u(x_q, y_q) - u_q = O(h^5)$. If one of the stencils is not smooth, we have $u(x_q, y_q) - u_q = O(h^3)$. This limit is the required order of accuracy for the reconstruction of moments for $\mathbf{P}^2$ based DGM. We can reconstruct the degrees of freedom in the same way by dividing the neighbors and using WENO reconstruction for $\mathbf{P}^3$ based DGM.

Runge-Kutta discretization parameters			
order	α_{il}	β_{il}	$\max\{\alpha_{il}/\beta_{il}\}$
2	1	1	1
	$\frac{1}{2}$ $\frac{1}{2}$	0 $\frac{1}{2}$	
3	1	1	1
	$\frac{3}{4}$ $\frac{1}{4}$	0 $\frac{1}{4}$	
	$\frac{1}{3}$ 0 $\frac{2}{3}$	0 0 $\frac{2}{3}$	

Table 1: TVD Runge-Kutta discretization parameters for orders 2 and 3

Now, equation (24) gives us the degrees of freedom for $\mathbf{P}^2$ based DGM. For a non-orthonormal basis, we define

$$D_i^j = |\Delta_0| \sum_q w_q u_q \psi_i^j((x_q, y_q)) \quad i = 1, \ldots, N_p - 1 \tag{30}$$

, $\mathbf{B}^j = \left[D_0^j - \hat{u}_0^j \left[M_{01}^j \right] \quad \ldots \quad D_{N_p-1}^j - \hat{u}_0^j \left[M_{0 N_p-1}^j \right] \right]^T$, $\mathbf{X}^j = \left[\hat{u}_0^j \ldots \hat{u}_{N_p-1}^j \right]^T$ and

$$\mathbf{A}^j = [A] = \begin{bmatrix} \left[M_{11}^j \right] & \cdots & \left[M_{1 N_p-1}^j \right] \\ \cdots & \cdots & \cdots \\ \left[M_{N_p-1 1}^j \right] & \cdots & \left[M_{N_p-1 N_p-1}^j \right] \end{bmatrix} \tag{31}$$

Here, the terms $\left[M_{mn}^j \right]$ are given by equation (9). Then the reconstructed degrees of freedom are given by $\mathbf{X}^j = (\mathbf{A}^j)^{-1} \mathbf{B}^j$. This formulation will work for any polynomial basis. Now, we can get the reconstructed polynomial solution in $\mathbf{I}_j$ by equation (3). We call this limiting procedure the compact subcell WENO limiting or CSWENO limiting in short. For solving a system of equations, we use this with a local characteristic field decomposition with the corresponding Jacobians in the x and y directions as explained in [6].

Now, the semi-discrete scheme given in equation (8) along with the limiter is discretized in time by using the TVD Runge-Kutta time discretization introduced in [22] which is described below briefly.

If $\{t^m\}_{m=0}^M$ is a partition of $[0, T]$ and $\Delta t^m = t^{m+1} - t^m$, $m = 0, \ldots, M - 1$, the time-marching algorithm reads as follows:

1) Set $u_h^0 = u_{0h}$, the initial condition;

2) For $m = 0, \ldots, M - 1$ compute u_h^{m+1} from u_h^m as follows:
(i) set $u_h^{(0)} = u_h^m$;
(ii) for $i = 1, 2, \ldots, d$ compute the intermediate functions:

$$u_h^{(i)} = \left[\sum_{l=0}^{i-1} \alpha_{il} u_h^{(l)} + \beta_{il} \Delta t^m L_h(u_h^{(l)}) \right]; \tag{32}$$

where d is the order of the time integration.
(iii) set $u_h^{m+1} = u_h^{(d)}$;

Some Runge-Kutta time discretization parameters are given in Table 1.

We have used the third order TVD Runge-Kutta time discretization for all our calculations.

	h	DG without limiter				DG with limiter			
		L_1 error	Order	L_∞ error	Order	L_1 error	Order	L_∞ error	Order
P^1	4/20	2.31E-02		4.14E-01		6.64E-03		8.35E-02	
	4/40	4.89E-03	2.24	8.47E-02	2.29	1.70E-03	1.97	2.21E-02	1.92
	4/80	1.01E-03	2.27	1.84E-02	2.20	4.37E-04	1.96	6.30E-03	1.81
	4/160	2.34E-04	2.11	4.76E-03	1.95	1.12E-04	1.96	1.82E-03	1.79
P^2	4/20	4.17E-04		9.39E-03		3.97E-04		9.66E-03	
	4/40	5.47E-05	2.93	1.34E-03	2.81	5.28E-05	2.91	1.82E-03	2.41
	4/80	7.59E-06	2.85	2.08E-04	2.69	7.32E-06	2.85	2.84E-04	2.68
	4/160	1.09E-06	2.80	4.14E-05	2.33	9.81E-07	2.90	4.02E-05	2.82
P^3	4/20	3.69E-05		2.27E-03		3.87E-05		8.23E-04	
	4/40	2.51E-06	3.88	1.63E-04	3.80	2.50E-06	3.95	6.08E-05	3.76
	4/80	1.73E-07	3.86	1.13E-05	3.85	1.63E-07	3.94	4.16E-06	3.87
	4/160	1.21E-08	3.84	8.28E-07	3.77	1.05E-08	3.96	2.83E-07	3.88

Table 2: 2D Burgers equation with the initial condition $u(x, y, 0) = 0.5 + \sin(\pi(x + y)/2)$, with periodic boundary conditions in both directions, $t = 0.5/\pi$, Triangular mesh with size h, L_1 and L_∞ errors for **P**^{1}, **P**^{2} and **P**^{3} based DGM

4   Results

In this section, we look at some of the results obtained to demonstrate the performance of the limiter (called the compact subcell WENO limiter or CSWENO limiter) described in Section 3. We used Gmsh 4.6.0 software [23] for the generation of meshes for all our calculations. All the results are obtained using RKDG method and the CSWENO limiter with a third order TVD Runge-Kutta scheme for time integration unless otherwise specified.

4.1   Accuracy Tests

We test the accuracy of the schemes with the CSWENO limiter for scalar and system problems for the two-dimensional test cases. We present the results of the accuracy tests using two-dimensional Burgers equations and the two-dimensional Euler equations. For all the accuracy tests conducted, we have marked all the cells as troubled cells. We used meshes which contain some triangles of irregular size as shown in Figure 5 for all our calculations to illustrate that the limiter retains the order of the scheme even for such meshes.

Example 1: We solve the two dimensional nonlinear scalar inviscid Burgers equation:

$$\frac{\partial u}{\partial t} + \frac{\partial (u^2/2)}{\partial x} + \frac{\partial (u^2/2)}{\partial y} = 0, \qquad (x, y) \in [-2, 2] \times [-2, 2] \qquad (33)$$

with the initial condition $u(x, y, 0) = 0.5 + \sin(\pi(x + y)/2)$, with periodic boundary conditions in both directions. The exact solution is smooth till $t = 0.5/\pi$. A sample mesh used is shown in Figure 5. The errors and numerical orders of accuracy are calculated at $t = 0.5/\pi$ by marking all the cells as troubled cells and are presented in Table 2. We can see that the CSWENO limiter maintains the order and magnitude of accuracy of the original DG method.

Example 2: We solve the two dimensional Euler equations:

$$\mathbf{U}_t + \mathbf{f}(\mathbf{U})_x + \mathbf{g}(\mathbf{U})_y = 0 \qquad (x, y) \in [0, 2] \times [0, 2] \qquad (34)$$

where $\mathbf{U} = (\rho, \rho u, \rho v, E)^T$, $\mathbf{f}(\mathbf{U}) = u\mathbf{U} + (0, p, 0, pu)^T$ and $\mathbf{g}(\mathbf{U}) = v\mathbf{U} + (0, 0, p, pv)^T$ with $p = (\gamma - 1)(E - \frac{1}{2}\rho(u^2 + v^2))$ and $\gamma = 1.4$. Here, ρ is the density, (u, v) is the velocity, E is the total energy and p is the pressure. The initial conditions are given by $\rho(x, y, 0) = 1 + 0.2\sin(\pi(x + y))$, $u(x, y, 0) = 0.7$, $v(x, y, 0) = 0.3$ and $p(x, y, 0) = 1.0$ and we use periodic boundary conditions in both directions. The exact solution is given by $\rho(x, y, t) = 1 + 0.2\sin(\pi(x + y - t))$, $u(x, y, t) = 0.7$, $v(x, y, t) = 0.3$ and $p(x, y, t) = 1.0$. A sample mesh used is shown in Figure 6. The errors in density and numerical
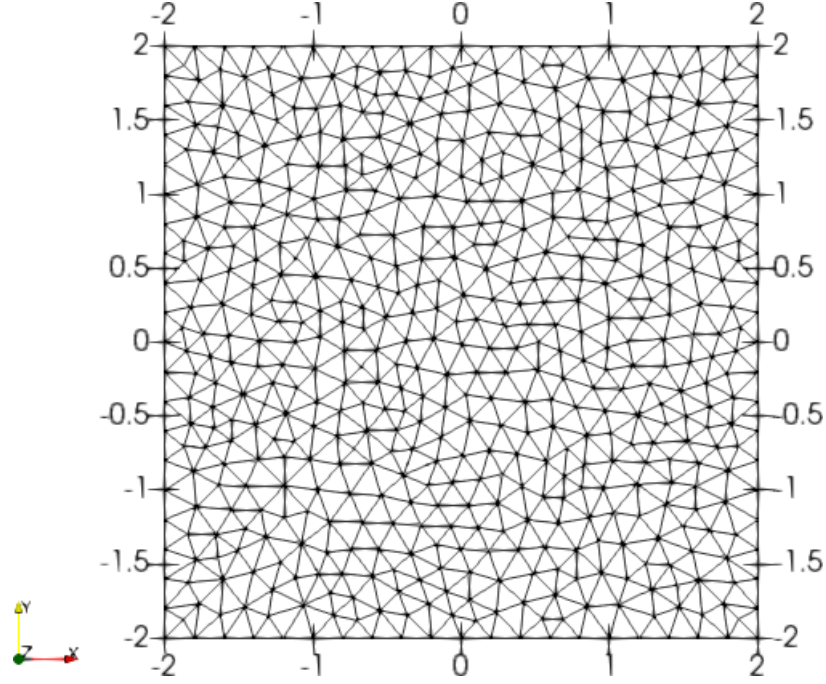
Figure 5: Burgers equation - Sample mesh where the mesh points on the boundary are uniformly distributed with cell length $h = 4/20$

orders of accuracy are calculated at $t = 2$ by marking all the cells as troubled cells and are presented in Table 3. Again, we can see that the CSWENO limiter maintains the order and magnitude of accuracy of the original DG method.

Example 3: We again solve the two dimensional Euler equations given by (34) for the Isentropic Euler Vortex problem suggested by Shu [24] as a test case in the domain $[0, 10] \times [-5, 5]$. The analytical solution is given by:

$\rho = \left(1 - \left(\frac{\gamma-1}{16\gamma\pi^2}\right)\beta^2 e^{2(1-r^2)}\right)^{\frac{1}{\gamma-1}}$, $u = 1 - \beta e^{(1-r^2)}\frac{y-y_0}{2\pi}$, $v = \beta e^{(1-r^2)}\frac{x-x_0-t}{2\pi}$, and $p = \rho^\gamma$, where $r = \sqrt{(x-x_0-t)^2 + (y-y_0)^2}$, $x_0 = 5$, $y_0 = 0$, $\beta = 5$ and $\gamma = 1.4$. We initialize with the analytical solution at $t = 0$ and use periodic boundary conditions at the edges of the domain in both directions. A sample mesh used is shown in Figure 7. The errors in density and numerical orders of accuracy are calculated at $t = 2$ by marking all the cells as troubled cells and are presented in Table 4. Again, we can see that the CSWENO limiter maintains the order and magnitude of accuracy of the original DG method.

4.2   Test Cases With Shocks

We now test the CSWENO (compact subcell WENO) limiter for problems with solutions having shocks.

Example 4: We solve the problem of shock interaction with entropy waves as proposed in [25] in the two-dimensional domain. We solve the 2D Euler equations with a moving shock interacting with sine waves in density in the domain $[0, 1] \times [0, 1]$ with the initial conditions given as $(\rho, u, v, p) = (3.857143, 2.629369, 0.0, 10.333333)$ for $x < 0.125$ and $(\rho, u, v, p) = (1.0 + 0.2\sin(16\pi x), 0, 0, 1)$ otherwise. Non reflecting boundary condition is applied at $x = 0$ and $x = 1$ and periodic boundary conditions are applied at the other two boundaries. The computed solution for density obtained at $t = 0.178$s using $h = 1/200$ at the $y = 0.5$ line while using the CSWENO limiter for $\mathbf{P}^1$, $\mathbf{P}^2$ and $\mathbf{P}^3$ based DGM is compared and plotted against the exact solution in Figure 8a. A surface color plot for density is shown in Figure 8b. We can see that good resolution is obtained in the solution for this problem using CSWENO

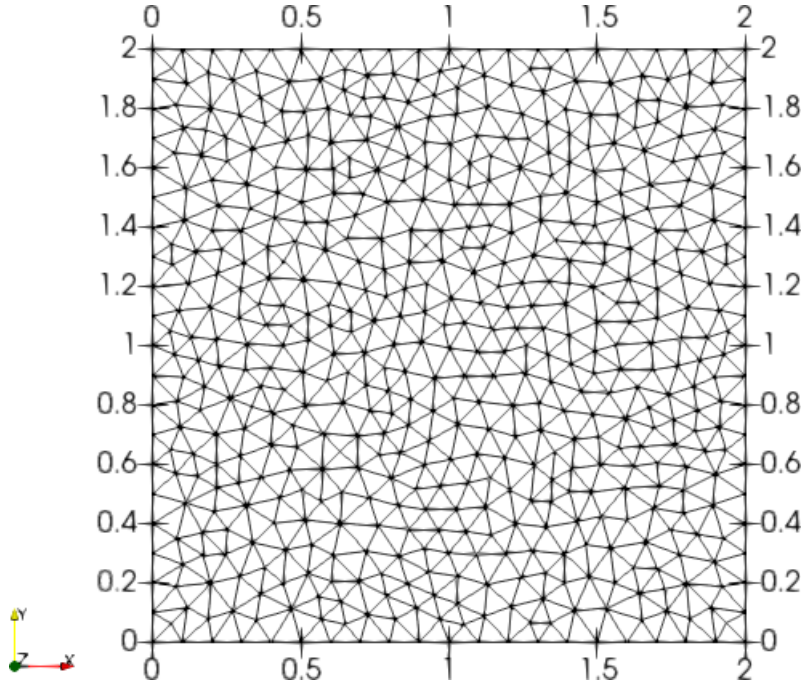|	h	DG without limiter				DG with limiter			
		L_1 error	Order	L_∞ error	Order	L_1 error	Order	L_∞ error	Order
$\mathbf{P}^1$	2/20	6.69E-03		2.87E-02		2.72E-03		6.95E-03	
	2/40	1.51E-03	2.15	7.58E-03	1.92	6.90E-04	1.98	1.81E-03	1.94
	2/80	3.13E-04	2.27	1.54E-03	2.30	1.74E-04	1.99	4.53E-04	2.00
	2/160	8.05E-05	1.96	3.57E-04	2.11	4.44E-05	1.97	1.17E-04	1.95
$\mathbf{P}^2$	2/20	1.02E-04		2.27E-03		8.21E-05		3.31E-03	
	2/40	1.15E-05	3.15	3.11E-04	2.87	1.03E-05	2.99	5.97E-04	2.47
	2/80	1.23E-06	3.22	4.66E-05	2.74	1.28E-06	3.01	9.19E-05	2.70
	2/160	1.55E-07	2.99	6.29E-06	2.89	1.69E-07	2.92	1.24E-05	2.89
$\mathbf{P}^3$	2/20	2.31E-06		4.25E-05		8.32E-07		7.24E-06	
	2/40	1.50E-07	3.95	3.25E-06	3.71	4.92E-08	4.08	5.31E-07	3.77
	2/80	9.91E-09	3.92	2.27E-07	3.84	2.99E-09	4.04	4.32E-08	3.62
	2/160	7.07E-10	3.81	1.52E-08	3.90	1.88E-10	3.99	2.93E-09	3.88

Table 3: 2D Euler equations with the initial condition $\rho(x, y, 0) = 1 + 0.2\sin(\pi(x + y))$, $u(x, y, 0) = 0.7$, $v(x, y, 0) = 0.3$ and $p(x, y, 0) = 1.0$, with periodic boundary conditions in both directions, $t = 2$, Triangular mesh with size h, L_1 and L_∞ errors for density with $\mathbf{P}^1$, $\mathbf{P}^2$ and $\mathbf{P}^3$ based DGM

Figure 6: 2D Euler equations with the initial condition $\rho(x, y, 0) = 1 + 0.2\sin(\pi(x + y))$, $u(x, y, 0) = 0.7$, $v(x, y, 0) = 0.3$ and $p(x, y, 0) = 1.0$ - Sample mesh where the mesh points on the boundary are uniformly distributed with cell length $h = 2/20$

	h	DG without limiter				DG with limiter			
		L_1 error	Order	L_∞ error	Order	L_1 error	Order	L_∞ error	Order
$\mathbf{P}^1$	10/20	4.57E-02		1.45E-01		4.35E-02		1.35E-01	
	10/40	1.00E-02	2.19	3.58E-02	2.02	1.10E-02	1.98	3.75E-02	1.85
	10/80	2.27E-03	2.14	1.11E-02	1.69	2.81E-03	1.97	1.01E-02	1.90
	10/160	6.00E-04	1.92	3.23E-03	1.78	7.07E-04	1.99	2.67E-03	1.92
$\mathbf{P}^2$	10/20	6.67E-03		9.93E-02		4.89E-03		8.39E-02	
	10/40	7.67E-04	3.12	1.38E-02	2.85	6.20E-04	2.98	1.13E-02	2.89
	10/80	9.26E-05	3.05	1.88E-03	2.88	7.91E-05	2.97	1.80E-03	2.65
	10/160	1.19E-05	2.96	3.12E-04	2.59	1.02E-05	2.95	2.73E-04	2.72
$\mathbf{P}^3$	10/20	8.11E-04		8.49E-03		8.27E-04		7.82E-03	
	10/40	5.03E-05	4.01	6.49E-04	3.71	5.28E-05	3.97	5.85E-04	3.74
	10/80	3.35E-06	3.91	5.28E-05	3.62	3.44E-06	3.94	4.53E-05	3.69
	10/160	2.32E-07	3.85	4.09E-06	3.69	2.32E-07	3.89	3.34E-06	3.76

Table 4: 2D Euler equations for the Isentropic Vortex problem with periodic boundary conditions in both directions, $t = 2$, Triangular mesh with size h, L_1 and L_∞ errors for density with $\mathbf{P}^1$, $\mathbf{P}^2$ and $\mathbf{P}^3$ based DGM
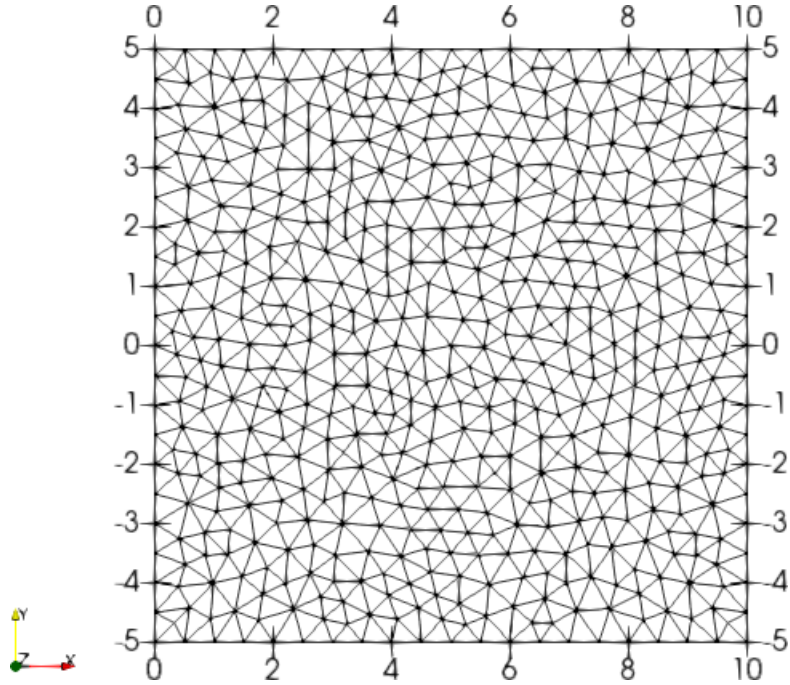

Figure 7: 2D Euler equations for Isentropic Vortex Problem - Sample mesh where the mesh points on the boundary are uniformly distributed with cell length $h = 10/20$
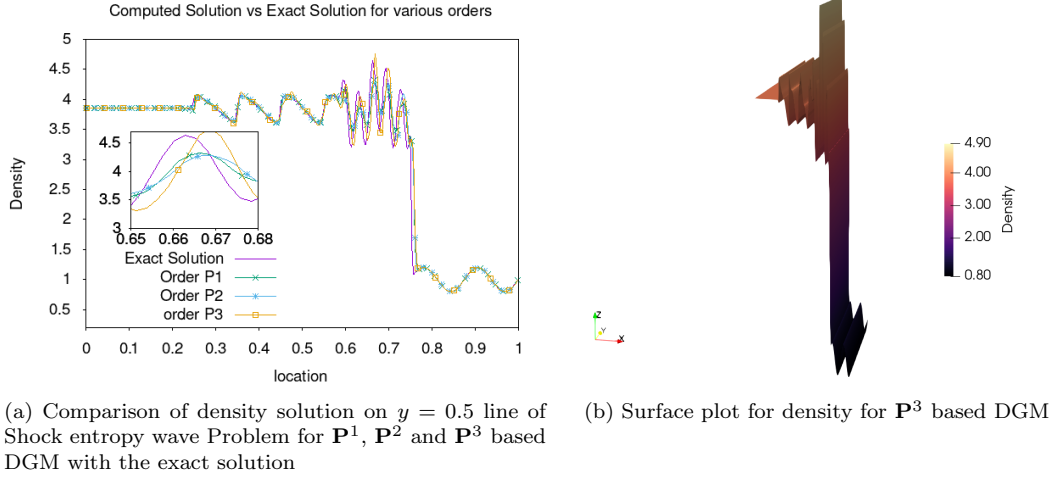
limiter.

(a) Comparison of density solution on $y = 0.5$ line of Shock entropy wave Problem for $\mathbf{P}^1$, $\mathbf{P}^2$ and $\mathbf{P}^3$ based DGM with the exact solution

(b) Surface plot for density for $\mathbf{P}^3$ based DGM

Figure 8: Solution of Shock entropy wave Problem at $t = 0.178$ with $h = 1/200$

Example 5: We solve the double Mach reflection problem as given in [26]. We solve the two-dimensional Euler equations in the computational domain $[0, 4] \times [0, 1]$. Initially, right moving Mach 10 shock is positioned at $x = 1/6, y = 0$ and it makes an angle 60^0 with the x-axis. For the bottom boundary, we impose the exact post shock conditions from $x = 0$ to $x = 1/6$ and for the rest of the x-axis, we use reflective boundary conditions. For the top boundary, we set conditions to describe the exact motion of a Mach 10 shock. We compute the solution upto time $t = 0.2$ for a mesh size of $h = 1/200$ which contains 370,046 triangles. A sample mesh of size $h = 1/20$ is shown in Figure 9. The density contours for the solution obtained using the CSWENO limiter for $\mathbf{P}^1$, $\mathbf{P}^2$ and $\mathbf{P}^3$ based DGM is shown in Figure 10. A zoom-in view of the density contours near the double Mach stem is shown in Figure 11 for $\mathbf{P}^1$, $\mathbf{P}^2$ and $\mathbf{P}^3$ based DGM. We can see that the solution obtained using CSWENO limiter is quite well comparable to the solution obtained in [26].
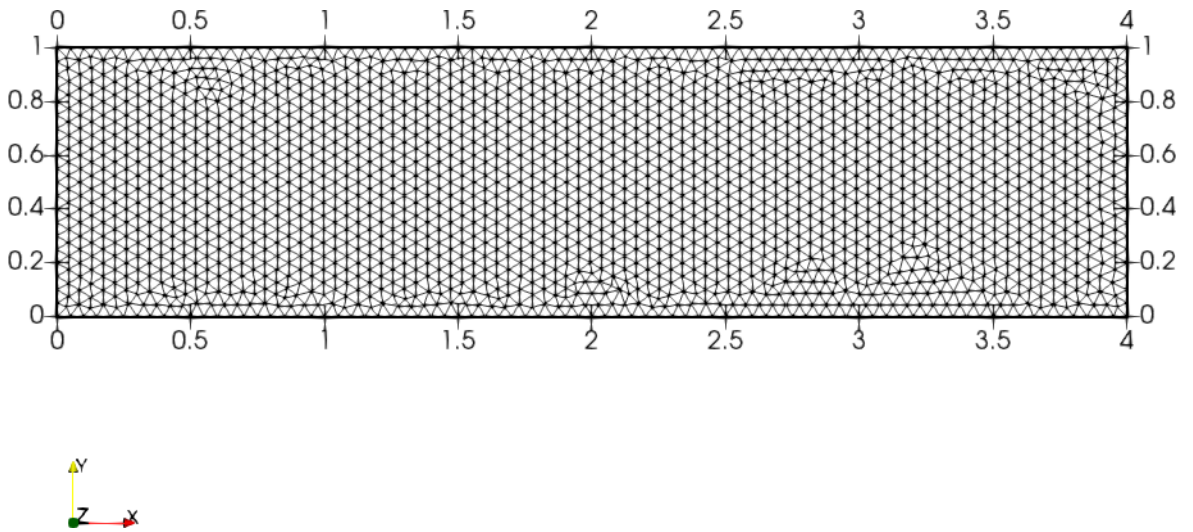

Figure 9: Double Mach reflection problem - Sample mesh where the mesh points on the boundary are uniformly distributed with cell length $h = 1/20$
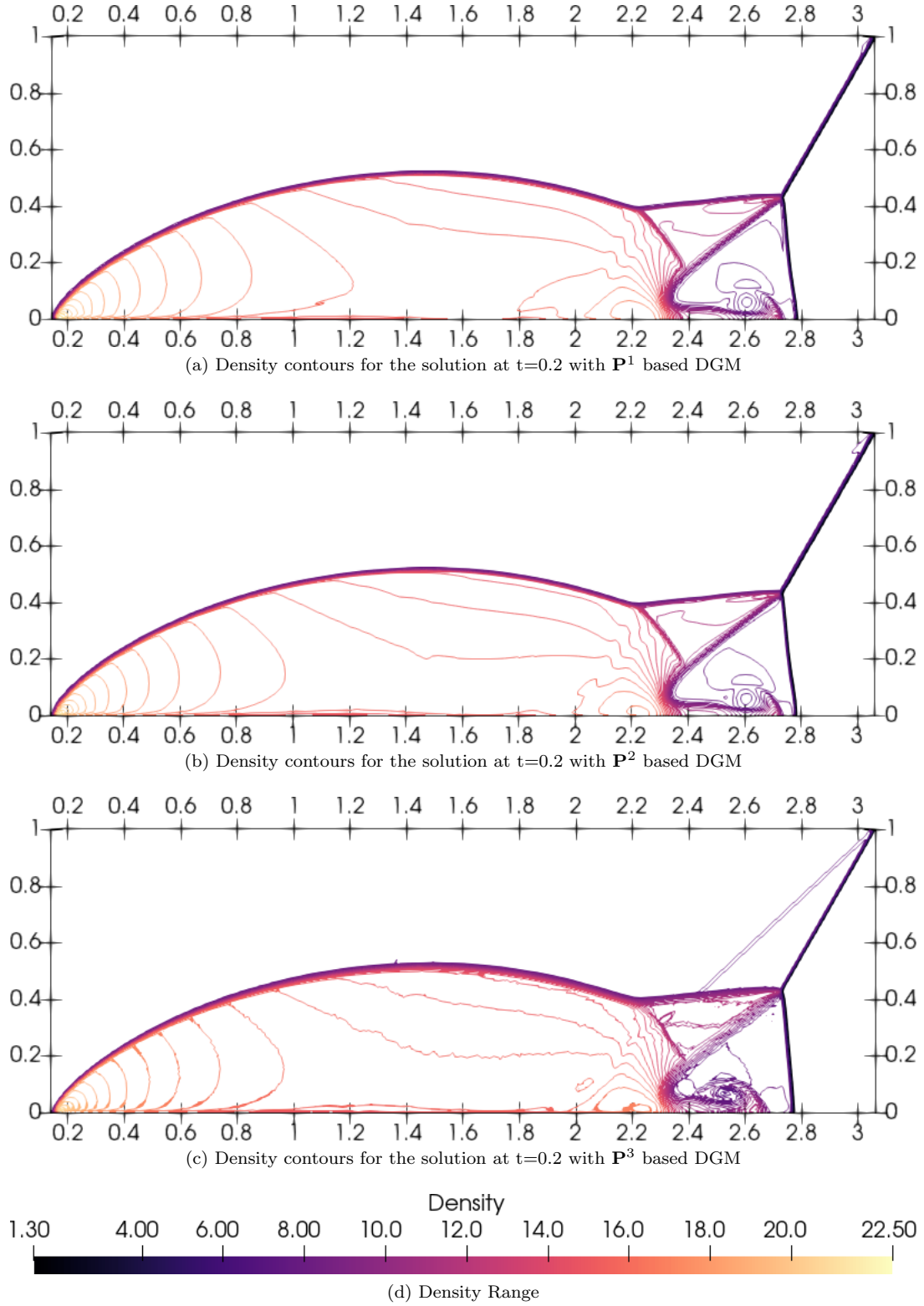
14

(a) Density contours for the solution at t=0.2 with $\mathbf{P}^1$ based DGM

(b) Density contours for the solution at t=0.2 with $\mathbf{P}^2$ based DGM

(c) Density contours for the solution at t=0.2 with $\mathbf{P}^3$ based DGM

(d) Density Range

Figure 10: 50 equally spaced density contours for Double Mach reflection solution using the CSWENO limiter with $h = 1/200$ for $\mathbf{P}^1$(top), $\mathbf{P}^2$(middle) and $\mathbf{P}^3$(bottom) based DGM
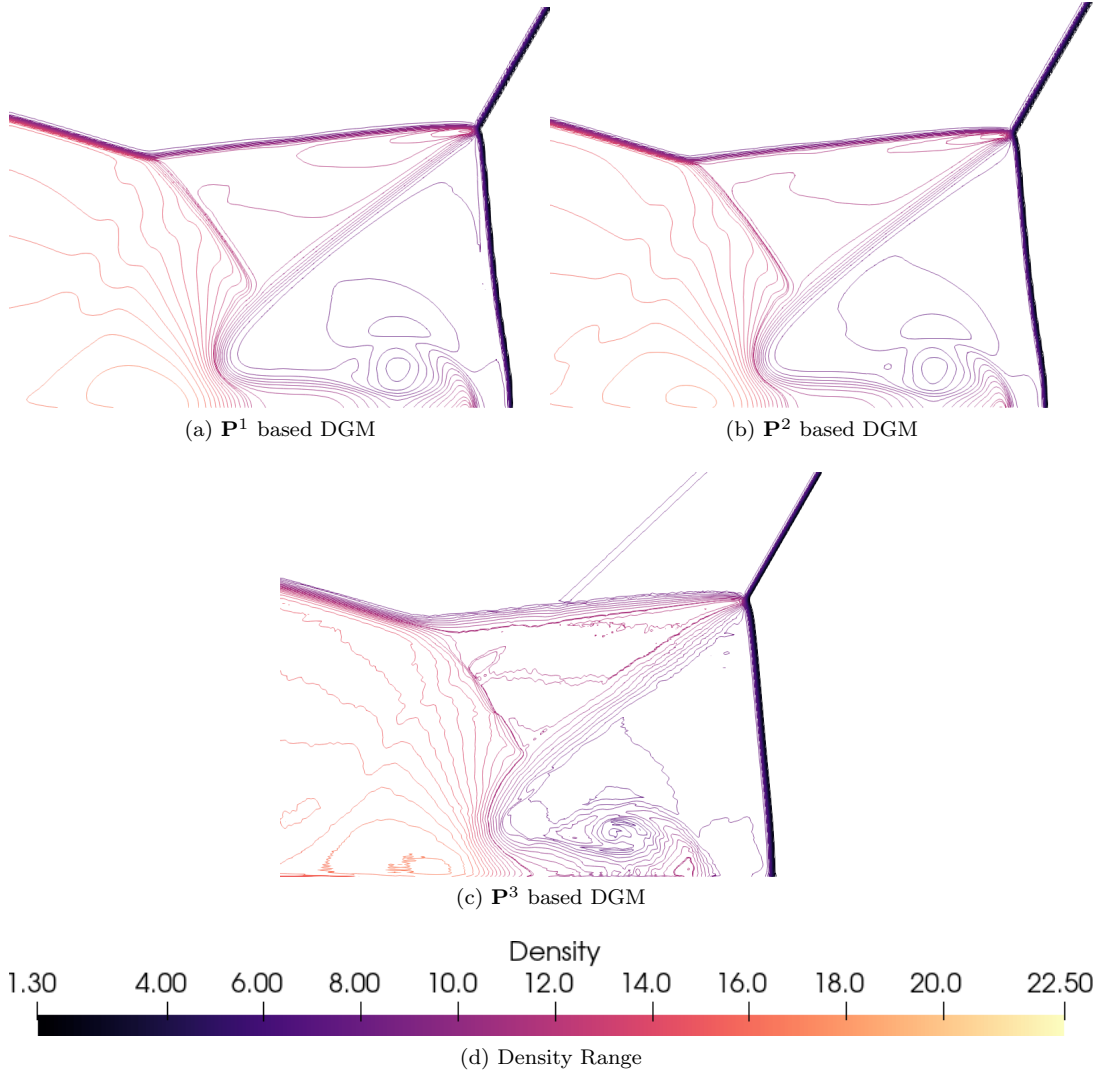
(a) $\mathbf{P}^1$ based DGM

(b) $\mathbf{P}^2$ based DGM

(c) $\mathbf{P}^3$ based DGM

Density

1.30   4.00   6.00   8.00   10.0   12.0   14.0   16.0   18.0   20.0   22.50

(d) Density Range

Figure 11: Density variation for Double Mach reflection solution using the CSWENO limiter for $\mathbf{P}^1$, $\mathbf{P}^2$ and $\mathbf{P}^3$ based DGM in the region $[2, 2.9] \times [0, 0.6]$ using 50 equally spaced contours

Example 6: As another test problem, we solve the flow over a forward facing step which is given in [26]. We solve the two-dimensional Euler equations in a flow set up which contains a right-going Mach 3 uniform flow in a wind tunnel of width 1 unit and length 4 units. The step height is 0.2 units and is located 1 units from the left hand end of the wind tunnel. The problem is initialized by a uniform, right-going Mach 3 flow. Reflective boundary conditions are applied along the walls of the tunnel and in-flow and out-flow boundary conditions are applied at the entrance and the exit, respectively. We compute the solution upto time $t = 4.0$ for a mesh size of $h = 1/100$ which contains 78982 triangles. A sample mesh of size $h = 1/20$ is shown in Figure 12. The density contours for the solution obtained using the CSWENO limiter for $\mathbf{P}^1$, $\mathbf{P}^2$ and $\mathbf{P}^3$ based DGM is shown in Figure 13. We can see that the solution obtained using CSWENO limiter is quite well comparable to the solution obtained in [26].
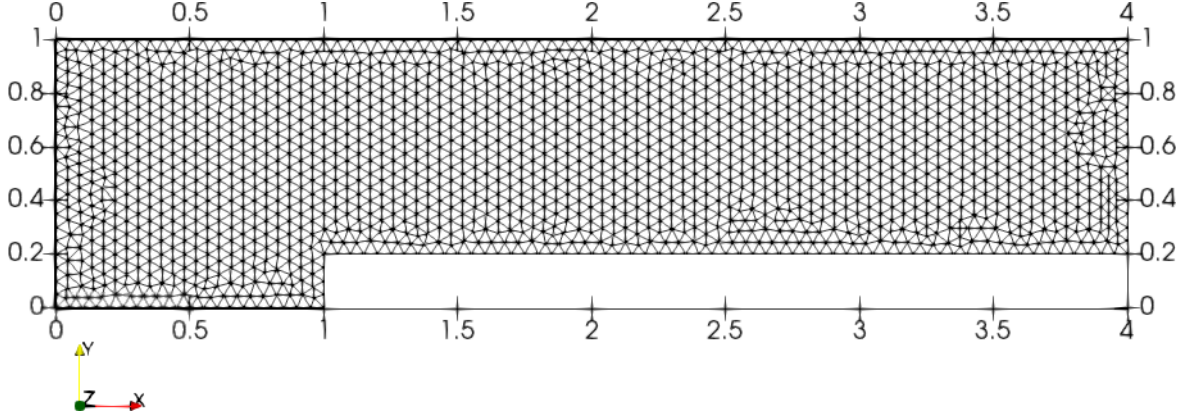
Figure 12: Flow over a forward facing step - Sample mesh where the mesh points on the boundary are uniformly distributed with cell length $h = 1/20$

Example 7: As another test case, we look at the 2D Riemann problem of gas dynamics which is one of the most extensively studied problem which also contains a lot of intricate flow structures. We solve the two-dimensional Euler equations in the domain $[0,1] \times [0,1]$ for 2D Riemann problem configurations (3) and (12) as given by the nomenclature in [27]. The initial conditions for configurations (3) and (12) are given respectively as

$$
(\rho, u, v, p)(x, y, 0) = \begin{cases} (1.5, 0, 0, 1.5) & \text{if } x \geq 0.5 \text{ and } y \geq 0.5 \\ (0.5323, 1.206, 0, 0.3) & \text{if } x < 0.5 \text{ and } y \geq 0.5 \\ (0.138, 1.206, 1.206, 0.029) & \text{if } x < 0.5 \text{ and } y < 0.5 \\ (0.5323, 0, 1.206, 0.3) & \text{otherwise} \end{cases} \tag{35}
$$

$$
(\rho, u, v, p)(x, y, 0) = \begin{cases} (0.5313, 0, 0, 0.4) & \text{if } x \geq 0.5 \text{ and } y \geq 0.5 \\ (1, 0.7276, 0, 1) & \text{if } x < 0.5 \text{ and } y \geq 0.5 \\ (0.8, 0, 0, 1) & \text{if } x < 0.5 \text{ and } y < 0.5 \\ (1, 0, 0.7276, 1) & \text{otherwise} \end{cases} \tag{36}
$$

We compute the solution upto time $t = 0.3$ for configuration (3) and till $t = 0.25$ for configuration (12). We use a mesh size of $h = 1/200$ which contains 92552 triangles. A sample mesh of size $h = 1/20$ is shown in Figure 14. The density contours for the solution obtained using the CSWENO limiter for $\mathbf{P}^1$, $\mathbf{P}^2$ and $\mathbf{P}^3$ based DGM are shown in Figures 15 and 16 respectively for configurations (3) and (12). We can see that the solution obtained using CSWENO limiter is quite well comparable to the solution obtained in [27].
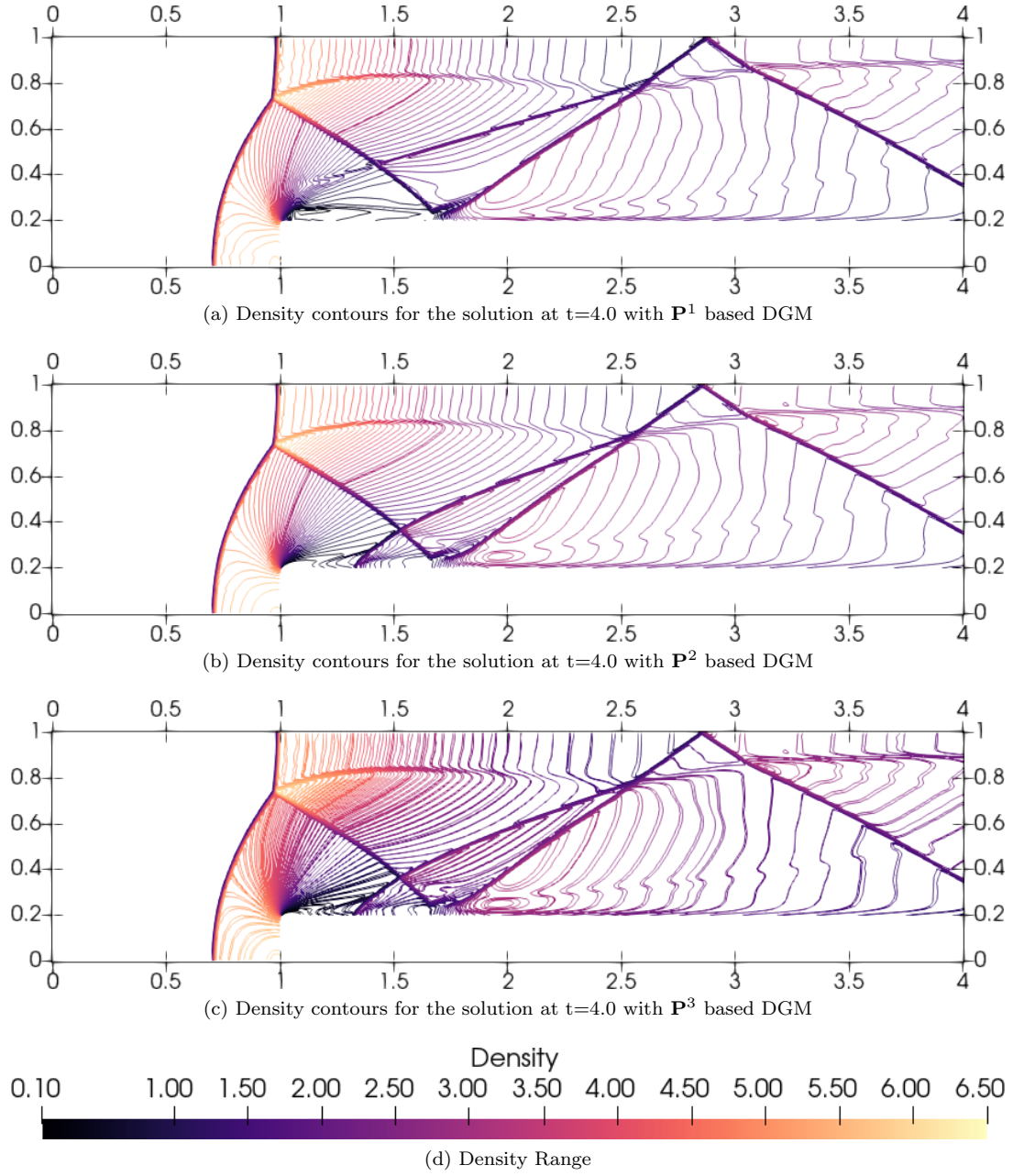
(a) Density contours for the solution at t=4.0 with $\mathbf{P}^1$ based DGM

(b) Density contours for the solution at t=4.0 with $\mathbf{P}^2$ based DGM

(c) Density contours for the solution at t=4.0 with $\mathbf{P}^3$ based DGM

(d) Density Range

Figure 13: 50 equally spaced density contours for solution of flow over a forward facing step using the CSWENO limiter with $h = 1/100$ for $\mathbf{P}^1$(top), $\mathbf{P}^2$(middle) and $\mathbf{P}^3$(bottom) based DGM
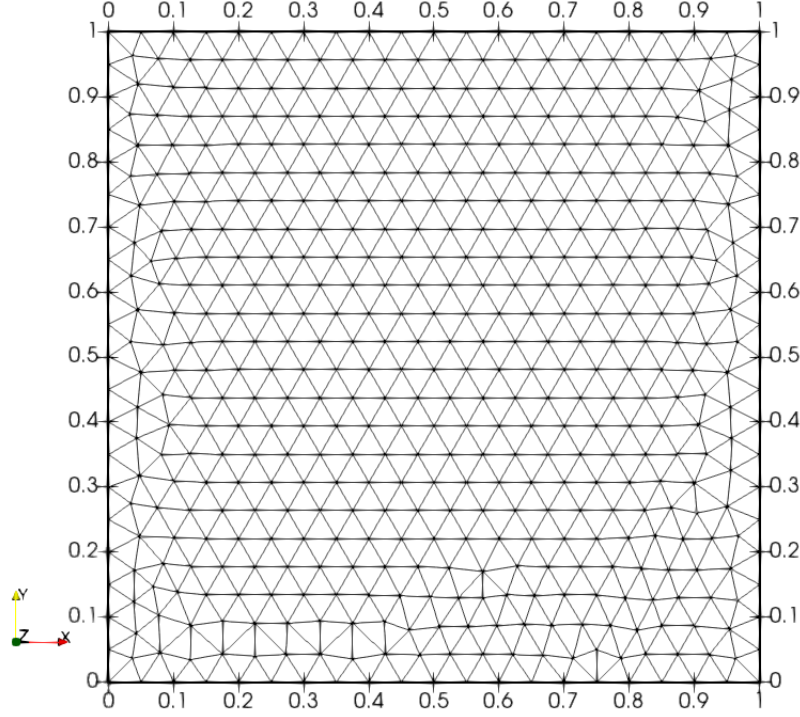
Figure 14: 2D Riemann problem of gas dynamics - Sample mesh where the mesh points on the boundary are uniformly distributed with cell length $h = 1/20$

5 Conclusions:

We have generalized the compact subcell WENO (CSWENO) limiting strategy for the solution of hyperbolic conservation laws using discontinuous Galerkin method proposed in [1] to unstructured triangular meshes. Using this strategy, we identify the troubled cells and use only the immediate neighbors by dividing them into subcells appropriately based on the order of accuracy of the scheme. These new cells are used for the WENO reconstruction. This formulation is different from the subcell limiting strategy of Dumbser et al [9] and Giri et al [10] which is much more accurate but quite complicated as they use subcells in an *a posteriori* limiting strategy. This limiting strategy can be used with any of the WENO reconstructions given in [11] (called type I WENO reconstruction), or [5] (called type II WENO reconstruction) or [12] (mixed reconstruction) or the more recent methods given in [13] and [2] by dividing the immediate neighbors appropriately. We use the WENO reconstruction given in [2] as it is quite simple in implementation and extension to higher orders is easy. We emphasize that our procedure works with any of the WENO reconstructions listed above by dividing the neighbors of the troubled cell as is required by the reconstruction. We termed this limiting procedure as the compact subcell WENO limiter (CSWENO limiter). We have tested the accuracy of this limiter using various standard test cases containing smooth solutions and calculating the numerical order of accuracy. We have also provided numerical results with shocks for standard test cases which are solutions of two-dimensional Euler equations to illustrate the performance of the limiter.

References

[1] S. R. Siva Prasad Kochi and M. Ramakrishna, "A compact subcell WENO limiting strategy using immediate neighbours for Runge-Kutta discontinuous Galerkin methods.," *International Journal of Computer Mathematics*, vol. 98, no. 3, pp. 608–626, 2021.

[2] J. Zhu and C.-W. Shu, "A new type of multi-resolution WENO schemes with increasingly higher order of accuracy on triangular meshes.," *Journal of Computational Physics*, vol. 392, pp. 19–33, 2019.
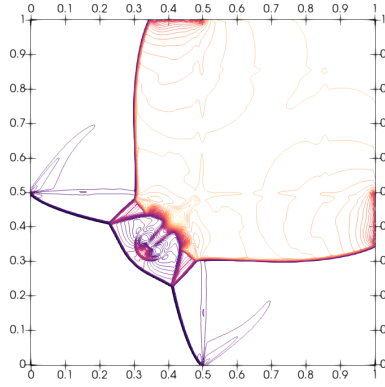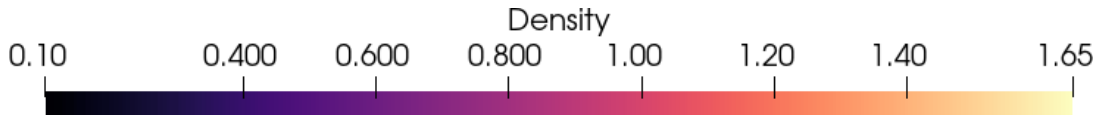
(a) Density contours for the solution at t=0.3 with $\mathbf{P}^1$ based DGM
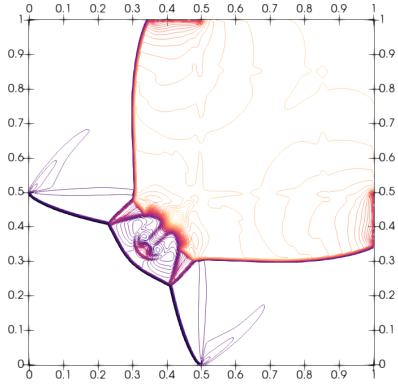
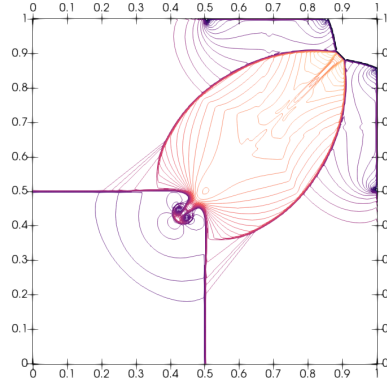(b) Density contours for the solution at t=0.3 with $\mathbf{P}^2$ based DGM
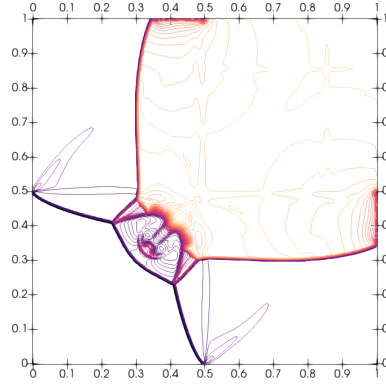
(c) Density contours for the solution at t=0.3 with $\mathbf{P}^3$ based DGM
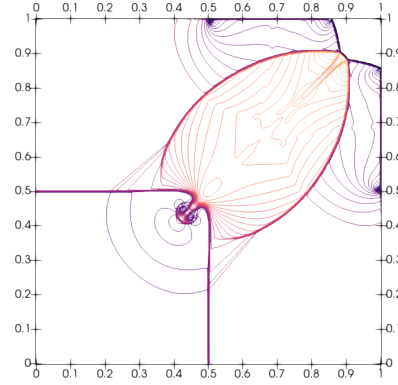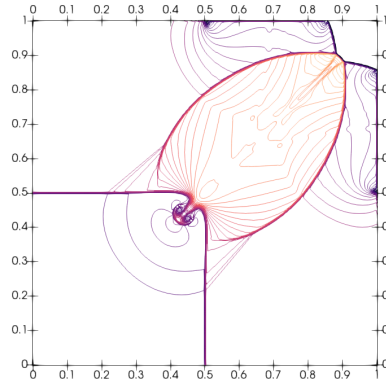
(d) Density Range

Figure 15: 50 equally spaced density contours for solution at $t = 0.3$ for 2D Riemann problem configuration 3 using the CSWENO limiter with $h = 1/200$ for $\mathbf{P}^1$, $\mathbf{P}^2$ and $\mathbf{P}^3$ based DGM
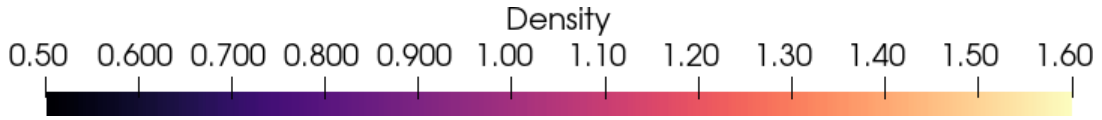
(a) Density contours for the solution at t=0.3 with $\mathbf{P}^1$ based DGM

(b) Density contours for the solution at t=0.3 with $\mathbf{P}^2$ based DGM

(c) Density contours for the solution at t=0.3 with $\mathbf{P}^3$ based DGM

(d) Density Range

Figure 16: 50 equally spaced density contours for solution at $t = 0.25$ for 2D Riemann problem configuration 12 using the CSWENO limiter with $h = 1/200$ for $\mathbf{P}^1$, $\mathbf{P}^2$ and $\mathbf{P}^3$ based DGM

[3] B. Cockburn and C.-W. Shu, "Runge-Kutta discontinuous Galerkin method for convection-dominated problems.," *J. Sci. Comput.*, vol. 16, pp. 173–261, 2001.

[4] J. Qiu and C.-W. Shu, "Runge-Kutta discontinuous Galerkin method using WENO limiters.," *SIAM J. Sci. Comput.*, vol. 26, pp. 907–929, 2005.

[5] J. Zhu, J. Qiu, C.-W. Shu, and M. Dumbser, "Runge-Kutta discontinuous Galerkin method using WENO limiters II: Unstructured meshes.," *Journal of Computational Physics*, vol. 227, pp. 4330–4353, 2008.

[6] J. Zhu, X. Zhong, C.-W. Shu, and J. Qiu, "Runge–Kutta discontinuous Galerkin method using a new type of WENO limiters on unstructured meshes.," *Journal of Computational Physics*, vol. 248, pp. 200–220, 2013.

[7] J. Zhu, X. Zhong, C.-W. Shu, and J. Qiu, "Runge-Kutta Discontinuous Galerkin Method with a Simple and Compact Hermite WENO Limiter on Unstructured Meshes.," *Commun. Comput. Phys.*, vol. 21, no. 3, pp. 623–649, 2017.

[8] H. Zhu, J. Qiu, and J. Zhu, "A simple, high-order and compact WENO limiter for RKDG method.," *Computers and Mathematics with Applications*, vol. 79, pp. 317–336, 2020.

[9] M. Dumbser and R. Loubere, "A simple robust and accurate a posteriori sub-cell finite volume limiter for the discontinuous Galerkin method on unstructured meshes.," *Journal of Computational Physics*, vol. 319, pp. 163–199, 2016.

[10] P. Giri and J. Qiu, "A high-order Runge-Kutta discontinuous Galerkin method with a subcell limiter on adaptive unstructured grids for two-dimensional compressible inviscid flows," *International Journal for Numerical Methods in Fluids*, vol. 91, no. 8, pp. 367–394, 2019.

[11] M. Dumbser and M. Kaser, "Arbitrary high order non-oscillatory finite volume schemes on unstructured meshes for linear hyperbolic systems.," *Journal of Computational Physics*, vol. 221, pp. 693–723, 2007.

[12] Y. Liu and Y.-T. Zhang, "A Robust Reconstruction for Unstructured WENO Schemes.," *J. Sci. Comput.*, vol. 54, pp. 603–621, 2013.

[13] J. Zhu and J. Qiu, "New finite volume weighted essentially nonoscillatory schemes on triangular meshes.," *SIAM J. Sci. Comput.*, vol. 40, no. 2, pp. A903–A928, 2018.

[14] C. Hu and C.-W. Shu, "Weighted essentially non-oscillatory schemes on triangular meshes.," *Journal of Computational Physics*, vol. 150, pp. 97–127, 1999.

[15] J. S. Hesthaven and T. Warburton, *Nodal Discontinuous Galerkin Methods: Algorithms, Analysis, and Applications.* Springer New York, 2008.

[16] L. Krivodonova, J. Xin, J.-F. Remacle, N. Chevaugeon, and J. Flaherty, "Shock detection and limiting with discontinuous Galerkin methods for hyperbolic conservation laws.," *Appl. Numer. Math.*, vol. 48, pp. 323–338, 2004.

[17] J. Qiu and C.-W. Shu, "A comparison of troubled-cell indicators for Runge-Kutta discontinuous Galerkin methods using weighted essentially nonoscillatory limiters.," *SIAM J. Sci. Comput.*, vol. 27, pp. 995–1013, 2005.

[18] D. M. Williams, L. Shunn, and A. Jameson, "Symmetric quadrature rules for simplexes based on sphere close packed lattice arrangements.," *Journal of Computational and Applied Mathematics*, vol. 266, pp. 18–38, 2014.

[19] T. Sonar, "On the construction of essentially non-oscillatory finite volume approximations to hyperbolic conservation laws on general triangulations: polynomial recovery, accuracy and stencil selection.," *Comput. Methods Appl. Mech. Engrg.*, vol. 140, pp. 157–181, 1997.

[20] G. Jiang and C.-W. Shu, "Efficient implementation of weighted ENO schemes.," *Journal of Computational Physics*, vol. 126, pp. 202–228, 1996.

[21] M. Castro, B. Costa, and W. S. Don, "High order weighted essentially non-oscillatory WENO-Z schemes for hyperbolic conservation laws.," *Journal of Computational Physics*, vol. 230, pp. 1766–1792, 2011.

[22] C.-W. Shu, "TVD time discretizations.," *SIAM J. Sci. Stat. Comput.*, vol. 9, pp. 1073–1084, 1988.

[23] C. Geuzaine and J.-F. Remacle, "Gmsh: a three-dimensional finite element mesh generator withbuilt-in pre- and post-processing facilities.," *International Journal for Numerical Methods in Engineering*, vol. 79, no. 11, pp. 1309–1331, 2009.

[24] C.-W. Shu, "Essentially non-oscillatory and weighted essentially non-oscillatory schemes for hyperbolic conservation laws.," *Lecture Notes in Mathematics, Springer*, vol. 1697, pp. 325–432, 1998.

[25] C.-W. Shu and S. Osher, "Effective implementation of essentially non-oscillatory shock-capturing schemes, II.," *Journal of Computational Physics*, vol. 83, pp. 32–78, 1989.

[26] P. Woodward and P. Colella, "The numerical simulation of two-dimensional fluid flow with strong shocks.," *Journal of Computational Physics*, vol. 54, pp. 115–173, 1984.

[27] P. D. Lax and X. D. Liu, "Solution of two-dimensional Riemann problem of gas dynamics by positive schemes.," *SIAM J. Sci. Comput.*, vol. 19, pp. 319–340, 1998.